ADVANCES IN ATMOSPHERIC SCIENCES, VOL. 34, FEBRUARY 2017, 181–198

• **Original Paper** •

On the Contrasting Decadal Changes of Diurnal Surface Temperature Range between the Tibetan Plateau and Southeastern China during the 1980s–2000s

Yang YANG[1,2,4] and Rongcai REN[*1,3]

[1]*State Key Laboratory of Numerical Modeling for Atmospheric Sciences and Geophysical Fluid Dynamics, Institute of Atmospheric Physics, Chinese Academy of Sciences, Beijing* 100029*, China*

[2]*Institute of Urban Meteorology, China Meteorological Administration, Beijing* 100089*, China*

[3]*Collaborative Innovation Center on Forecast and Evaluation of Meteorological Disasters and KLME, Nanjing University of Information Science and Technology, Nanjing* 210044*, China*

[4]*University of Chinese Academy of Sciences, Beijing* 100049*, China*

(Received 30 March 2016; revised 7 September 2016; accepted 12 October 2016)

ABSTRACT

The diurnal surface temperature range (DTR) has become significantly smaller over the Tibetan Plateau (TP) but larger in southeastern China, despite the daily mean surface temperature having increased steadily in both areas during recent decades. Based on ERA-Interim reanalysis data covering 1979–2012, this study shows that the weakened DTR over TP is caused by stronger warming of daily minimum surface temperature (Tmin) and a weak cooling of the daily maximum surface temperature (Tmax); meanwhile, the enhanced DTR over southeastern China is mainly associated with a relatively stronger/weaker warming of Tmax/Tmin. A further quantitative analysis of DTR changes through a process-based decomposition method—the Coupled Surface–Atmosphere Climate Feedback Response Analysis Method (CFRAM)—indicates that changes in radiative processes are mainly responsible for the decreased DTR over the TP. In particular, the increased low-level cloud cover tends to induce the radiative cooling/warming during daytime/nighttime, and the increased water vapor helps to decrease the DTR through the stronger radiative warming during nighttime than daytime. Contributions from the changes in all radiative processes (over −2°C) are compensated for by those from the stronger decreased surface sensible heat flux during daytime than during nighttime (approximately 2.5°C), but are co-contributed by the changes in atmospheric dynamics (approximately −0.4°C) and the stronger increased latent heat flux during daytime (approximately −0.8°C). In contrast, the increased DTR over southeastern China is mainly contributed by the changes in cloud, water vapor and atmospheric dynamics. The changes in surface heat fluxes have resulted in a decrease in DTR over southeastern China.

Key words: Tibetan Plateau, diurnal surface temperature range, decadal change, CFRAM

Citation: Yang, Y., and R. C. Ren, 2017: On the contrasting decadal changes of diurnal surface temperature range between the Tibetan Plateau and southeastern China during the 1980s–2000s. *Adv. Atmos. Sci.*, **34**(2), 181–198, doi: 10.1007/s00376-016-6077-z.

1. Introduction

The diurnal temperature range (DTR), defined as the difference between the daily maximum surface temperature (Tmax) and minimum surface temperature (Tmin), is an important indicator of climate change against the background of global warming. This is because the long-term changes in Tmax and Tmin can provide additional information on top of the mean surface temperature changes, of the climate changes and climate processes (Braganza et al., 2004). Since the middle of the 20th century, the DTR has decreased in most parts of the world, with significant regional and seasonal features (Karl et al., 1993; Easterling et al., 1997). The narrowing of the DTR has mostly resulted from the relatively stronger surface Tmin warming than Tmax warming, while in some places the Tmin warming is accompanied by Tmax cooling (Karl et al., 1993). Previous studies have also reported a significant decrease in DTR over China in the past several decades (Dai et al., 1999; Liu et al., 2004; Zhou et al., 2010; Xia, 2013; Shen et al., 2014). Specifically, the DTR over China exhibited a rapid decrease [−0.25°C (10 yr)$^{-1}$] from 1960 to 1990, due to an increase in Tmin and slight decrease in Tmax (Shen et al., 2014), but a slight increase during the 1990s because of the similar pace of Tmax and Tmin warming (Liu et al., 2004). As a result, the area-mean DTR

* Corresponding author: Rongcai REN
Email: rrc@lasg.iap.ac.cn

over China during 1962–2011 shows a much lower decreasing rate [0.16°C (10 yr)$^{-1}$] than that during 1960–90 (Shen et al., 2014). In addition, the DTR over China has also exhibited significant spatial and seasonal variation, showing a relatively stronger decrease in the winter season or in northern China than that in summer or in southern China (Xia, 2013; Shen et al., 2014).

The Tibetan Plateau (TP) is the world highest ridge and covers a region about a quarter of the size of the Chinese territory. The dynamic and thermodynamic forcing effects of the TP are crucial to the formation of the Asian monsoon and the climate pattern in Asia (Duan and Wu, 2005, 2008; Wu et al., 2012; Wang et al., 2014). The changes over the TP may also have profound influences on the global climate beyond East Asia (Yanai and Wu, 2006; Wu et al., 2007, Kang et al., 2010; Yang et al., 2014; Ren et al., 2014). Previous studies report that the TP experienced a significant warming at a rate of 0.16°C (10 yr)$^{-1}$ during the period 1955–96, which is much higher than that for the Northern Hemisphere and for the same latitudinal zone during the same period (Liu and Chen, 2000; Oku et al., 2006; Duan and Xiao, 2015). Under this stronger long-term warming over TP, however, a distinct decreasing of the DTR [−0.19°C (10 yr)$^{-1}$] was observed during 1961–2005 (Duan et al., 2006; Duan and Wu, 2006; You et al., 2008), attributed to the greater warming in Tmin [0.45°C (10 yr)$^{-1}$] than that in Tmax [0.26°C (10 yr)$^{-1}$] (Shen et al., 2014).

Many previous studies have suggested that the increase in cloud cover is one of the main causes for the reduction of the DTR over the TP, due to changes in the surface energy and hydrological balance (Karl et al., 1993). Specifically, the increased cloud cover leads to lower Tmax through reflecting incident shortwave radiation during daytime, but results in higher Tmin through intercepting the outgoing longwave radiation during nighttime (Karl et al., 1993; Dai et al., 1999; Stone and Weaver, 2003; Duan et al., 2006). However, You et al. (2016) found that the correlation between the DTR and the cloud cover over the TP varies temporally and spatially. Xia (2013) indicated that the decrease in total cloud cover across China during 1954–2009 is largely inconsistent with the general reduction of the DTR over China. The secondary damping effect of increased evaporation due to the increased soil moisture and precipitation have been suggested as another main cause of the reduced DTR over the TP (Dai et al., 1999; You et al., 2016). Nevertheless, increased water vapor in the atmosphere may not yield any further effect on the DTR, due to the warming effect on both Tmax and Tmin (Dai et al., 1999). Other previous studies have indicated possible influences on the long-term changes of the DTR over the TP, from temperature advection by changes in the atmospheric circulation (You et al., 2016) and local effects from urbanization, land-use and vegetation (Easterling et al., 1997; Collatz et al., 2000; Ren and Zhou, 2014). However, a consensus is still lacking with respect to the physical processes mainly responsible for the changes in the DTR over the TP in recent decades. This is crucial to our understanding of the surface-atmosphere energy balance over the TP, as well as the regional and global climate effects of the TP. In particular, the lack of consensus on the long-term changes of the DTR over the TP calls for a systematic assessment of the changes in various physical processes and their possible contributions to the changes in the DTR and the surface–atmosphere energy balance over the TP.

Under the framework of the energy balance within the coupled surface–atmosphere system, Lu and Cai (2009) and Cai and Lu (2009) developed a process-based decomposition method called CFRAM (Coupled Surface–Atmosphere Climate Feedback Response Analysis Method). CFRAM can quantitatively attribute the total temperature changes to the changes in individual radiative processes, including external forcing (e.g. CO_2 and incident solar radiation), surface albedo, cloud, water vapor feedback, and non-radiative processes including surface sensible and latent heat flux, and dynamic processes in the surface–atmosphere coupled system. CFRAM was originally used for evaluating the climate feedbacks under global warming (Cai and Tung, 2012; Sejas et al., 2014; Yang et al., 2016). Recently, CFRAM has been adopted for analyzing the surface temperature responses over the tropical Pacific and North America associated with El Niño–Southern Oscillation (ENSO) (Deng et al., 2012), and ENSO-related sea surface temperature anomalies in the Indian Ocean (Ren et al., 2016). CFRAM has also been employed in the attribution of surface temperature biases (Park et al., 2014; Yang et al., 2015; Liu et al., 2015) and atmospheric temperature biases in climate models (Ren et al., 2015; Yang and Ren, 2015).

The purpose of the present study is to re-examine the long-term change in the DTR over the TP by using a longer time series, and apply CFRAM to perform an attribution analysis of the changes. We provide quantitative evidence indicating the relative contributions of the decadal changes in various physical processes, including external forcing and individual radiative and non-radiative feedback processes, to the changes in the DTR over the TP and southeastern China. This study will benefit our understanding of the decadal changes in surface temperature and the surface energy-balance processes over the TP, as well as help us to understand the related climate effects of the TP under global warming.

The remainder of the paper is organized as follows. Section 2 briefly introduces the data used and the application of CFRAM, including its mathematical formulation. Section 3 demonstrates the long-term changes in the DTR over the TP and southeastern China. The decomposition results and the partial contributions of individual processes to the long-term changes in the DTR are analyzed in section 4. The final section provides concluding remarks.

2. Data and method

2.1. *Data*

This study adopts the 6-hourly variables from the ERA-Interim dataset (Dee et al., 2011), which covers the period from 1979 to the present day, and has a horizontal resolution of $1.5^\circ \times 1.5^\circ$ and 37 pressure levels ranging from 1000 hPa

to 1 hPa. We define the daily Tmin/Tmax over the TP and southeastern China as the surface temperature at 0000/0600 UTC.

The quality of the ERA-Interim dataset, including the consistency among various variables, has been systematically evaluated in previous studies. In particular, it has been indicated that ERA-Interim has the best overall performance among all reanalysis datasets in representing the monthly temperature and daily temperature extremes over the TP, based on comparison with observations at 63 China Meteorological Administration observational stations over the TP (Mao et al., 2010; Wang and Zeng, 2012). By comparing the long-term trend in reanalysis datasets with the observed temperature trend, Sun et al. (2013) indicated that, for the long-term warming trend over the TP, ERA-Interim gives the best estimation relative to several other reanalysis datasets, despite weaker magnitudes relative to observations. You et al. (2013) indicated that the DTR changes over China from ECMWF reanalysis data exhibit a relatively smaller bias (<0.4%) and a higher positive correlation with observations (approximately 0.7) than that from NCEP–NCAR reanalysis data. Decker et al. (2012) evaluated several reanalysis products based on *in situ* measurements at 33 flux tower sites on different timescales, and found that ERA-Interim generally exhibits the lowest bias in representing the six-hourly temperature fields. As for other variables, Liang (2012) indicated that, compared with other reanalyses (JRA-25 and NCEP final reanalysis data), the atmospheric water vapor content over the TP from ECMWF reanalysis data agrees much better with ground-based GPS observational data. Finally, validation with ground-measured datasets indicate that the latent and sensible heat fluxes from ERA-Interim are also generally the best, with the lowest RMSEs among five products (Shi and Liang, 2014).

2.2. *Method*

For a surface-atmosphere column, CFRAM describes the difference (Δ) of the total energy balance between two climate states as

$$\Delta S - \Delta R + \Delta Q_{\mathrm{NRad}} = 0\ . \tag{1}$$

Here, we consider the decadal change of Tmax/Tmin and thus the DTR changes as the difference between the latter decade (the 2000s, 2000–09) and the earlier decade (the 1980s, 1980–89). ΔR and ΔS are the difference in the divergence of the longwave radiation flux and the convergence of the shortwave radiation flux, respectively, between the 2000s and 1980s. ΔQ_{NRad} represents the difference between the 1980s and the 2000s in the convergence of the total energy flux, mainly due to surface sensible heat flux (ΔQ_{SH}), surface latent heat flux (ΔQ_{LH}), the dynamic processes (ΔQ_{dyn}) involving net energy convergence at the surface (i.e., surface energy transport and energy storage), and the dynamical processes in the atmosphere on all scales, including turbulence, convection and large-scale atmospheric motions:

$$\Delta Q_{\mathrm{NRad}} = \Delta Q_{\mathrm{SH}} + \Delta Q_{\mathrm{LH}} + \Delta Q_{\mathrm{dyn}}\ . \tag{2}$$

Based on the linear approximation in CFRAM, the nonlinear interactions among various radiative feedback processes are negligible. Thus, ΔS and ΔR can be linearly decomposed into the sum of partial energy perturbations due to the changes in individual radiative processes, such as radiative forcing due to CO_2 concentration ($\Delta F_{\mathrm{CO_2}}$), surface albedo (α), cloud (c), water vapor (wv), and that due to the temperature changes (ΔT) between the 1980s and 2000s:

$$\begin{cases} \Delta S \approx \Delta F_{\mathrm{CO_2}} + \Delta S_{\alpha} + \Delta S_{\mathrm{c}} + \Delta S_{\mathrm{wv}}\ , \\ \Delta R \approx \Delta R_{\mathrm{c}} + \Delta R_{\mathrm{wv}} + \left(\dfrac{\partial R}{\partial T}\right)\Delta T, \end{cases} \tag{3}$$

where $\partial R/\partial T$ is the Planck feedback matrix whose jth column corresponds to the vertical profile of the radiative energy perturbation due to 1-K warming at the jth layer from the 1980s to the 2000s. Thus, $(\partial R/\partial T)\Delta T$ represents the difference in divergence of the longwave radiation energy flux due to the changes in temperature itself. To obtain the radiative energy perturbations and the Planck feedback matrix in Eq. (3), the Fu–Liou radiative transfer model (Fu and Liou, 1992, 1993) is used in CFRAM. A more detailed description of the calculation of individual processes can be found in Yang et al. (2015). After substituting Eqs. (2) and (3) into Eq. (1), rearranging the terms and then multiplying both sides of the equation by $(\partial R/\partial T)^{-1}$, we obtain

$$\Delta T \approx \left(\frac{\partial R}{\partial T}\right)^{-1} [\Delta F_{\mathrm{CO_2}} + \Delta S_{\alpha} + \Delta(S-R)_{\mathrm{c}} + \Delta(S-R)_{\mathrm{wv}} + \Delta Q_{\mathrm{SH}} + \Delta Q_{\mathrm{LH}} + \Delta Q_{\mathrm{dyn}}]. \tag{4}$$

Based on Eq. (4), the changes in the local Tmax and Tmin at each grid point between the 1980s and 2000s can be directly attributed to the changes in the radiative processes associated with [left to right in Eq. (4)] CO_2, surface albedo, cloud, water vapor feedbacks, and non-radiative processes including surface sensible heat-flux, surface latent heat-flux, dynamic processes at the surface and that in the atmosphere. The mean CO_2 concentration for the 2000s is a globally uniform value of 376.6 ppm, which is an increase of more than 30 ppm relative to that for the 1980s (345.4 ppm) (from NOAA's Earth System Research Laboratory Global Monitoring Division: http://www.esrl.noaa.gov/gmd/index.html).

3. Contrasting the decadal changes in the DTR between the TP and southeastern China during the 1980s–2000s

Figures 1a and c show the time series of the area-averaged annual surface temperature (red) and DTR (blue) over the TP and southeastern China in the past decades since 1979. The TP and southeastern China domains are (20°–40°N, 78°–103°E) and (22°–32°N, 105°E to the southeast coast of China), respectively, as marked by the blue boxes in Fig. 2c. It is clear that, while the daily mean surface temperature over the TP is warming up significantly

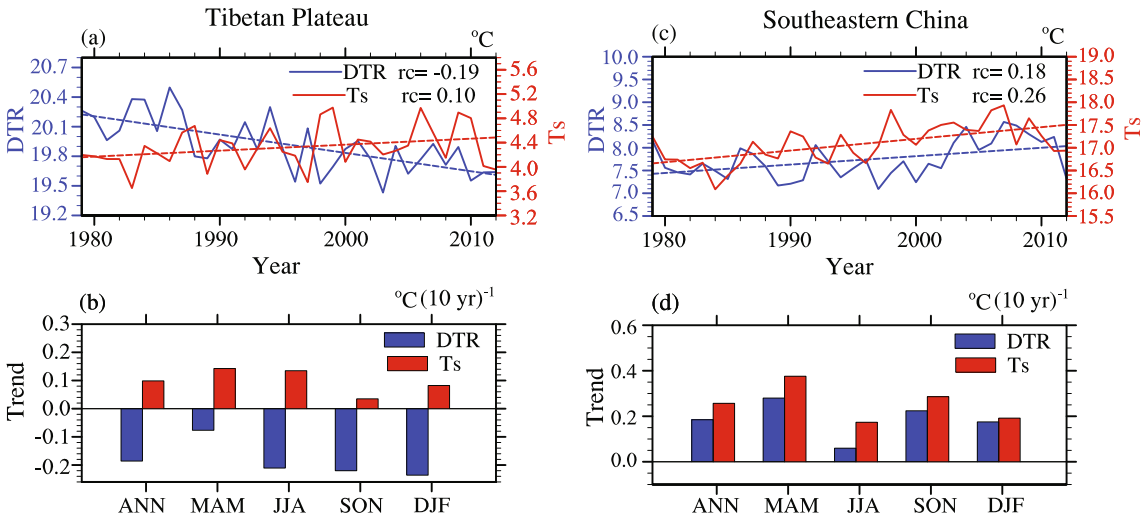

Fig. 1. (a) Time series of annual mean surface temperature (red; units: °C) and its diurnal temperature range (blue) over the Tibetan Plateau during 1979–2012. The dashed lines represent the linear fit. (b) Linear trend [units: °C (10 yr)$^{-1}$] of annual mean and seasonal surface temperature (red bars) and DTR (blue bars) over the Tibetan Plateau during 1979–2012. (c, d) As in (a, b) but over southeastern China.

[0.10°C (10 yr)$^{-1}$], the annual mean DTR is decreasing, by about 0.5°C since 1979, and at a rate of −0.19°C (10 yr)$^{-1}$, which is quite comparable with that [−0.20°C (10 yr)$^{-1}$] based on longer observational data records (1961–2013) (You et al., 2015). Opposite long-term changes between surface temperature and the DTR are also clear in all four seasons (Fig. 1b). In particular, the relatively stronger surface temperature warming in spring (March–April–May, MAM) is accompanied by a relatively weaker DTR decrease than in other seasons; and the DTR decrease is strongest in winter (December–January–February, DJF), at a rate of about −0.23°C (10 yr)$^{-1}$.

In contrast, the long-term surface warming [0.26°C (10 yr)$^{-1}$] over southeastern China is accompanied by an increased DTR [0.18°C (10 yr)$^{-1}$] since 1979 (Fig. 1c). The increase in the DTR over southeastern China since 1982 was also indicated in Xia (2013). It can be seen from Fig. 1d that the increase in surface temperature exhibits a similar seasonality to that of the DTR increase, both showing a fastest increase in spring (MAM), when the DTR rate of increase is over 0.2°C (10 yr)$^{-1}$, which is much higher than that obtained from observation [0.04°C (10 yr)$^{-1}$] (Xia, 2013).

Figure 2 shows the spatial distributions of the linear trends of Tmax (left), Tmin (middle) and DTR (right), during the period 1979–2012, on an annual and seasonal basis, respectively. It is evident that the long-term decrease in the annual mean DTR over the entire TP generally results from the warming of Tmin and cooling of Tmax (Figs. 2a–c). The most dramatic decrease in the DTR [exceeding −0.8°C (10 yr)$^{-1}$] lies over the northeast and central TP, also shown in You et al. (2016) based on observation. In contrast, the increase in the DTR over southeastern China is characterized by more remarkable warming during daytime than during nighttime, and the strongest increase in the DTR [over 0.2°C (10 yr)$^{-1}$] mainly exists over Guangdong and Guangxi provinces (Figs. 2a–c).

Comparing the DTR changes over the TP among different seasons, it is found that the stronger DTR decrease in the winter season is due to the remarkable cooling of Tmax and weak warming of Tmin. The strongest DTR trend is located over the northeast TP in autumn (September–October–November, SON) but over the southwest TP in DJF (Figs. 2l and o). However, associated with the stronger DTR increase in MAM across southeastern China, the warming trends of Tmax and Tmin are both stronger than in other seasons, particularly that of Tmax, showing a warming trend of 0.8°C (10 yr)$^{-1}$ (Figs. 2d and e). It is also noted that, unlike that in MAM and SON, the significant positive DTR trends in JJA and DJF only appear within Guangdong and Guangxi provinces (Figs. 2i and o), corresponding to the relative weaker DTR trend shown in Fig. 1d.

4. Quantitative attribution analysis of the decadal DTR changes over the TP and southeastern China

4.1. *Validation of the DTR changes in CFRAM*

Before the quantitative attribution analysis of the Tmax, Tmin and DTR, we first show in Figs. 3a–c their long-term changes in terms of the annual mean differences between the 2000s and 1980s. Relative to that in the 1980s, the Tmax in the 2000s becomes lower over most parts of the TP, whereas the Tmin mostly becomes higher. This directly leads to the decreased DTR over most parts of the TP, except the western TP (over −2°C), which is in agreement with the linear trend of the DTR in Fig. 2c. In contrast, a stronger warming of

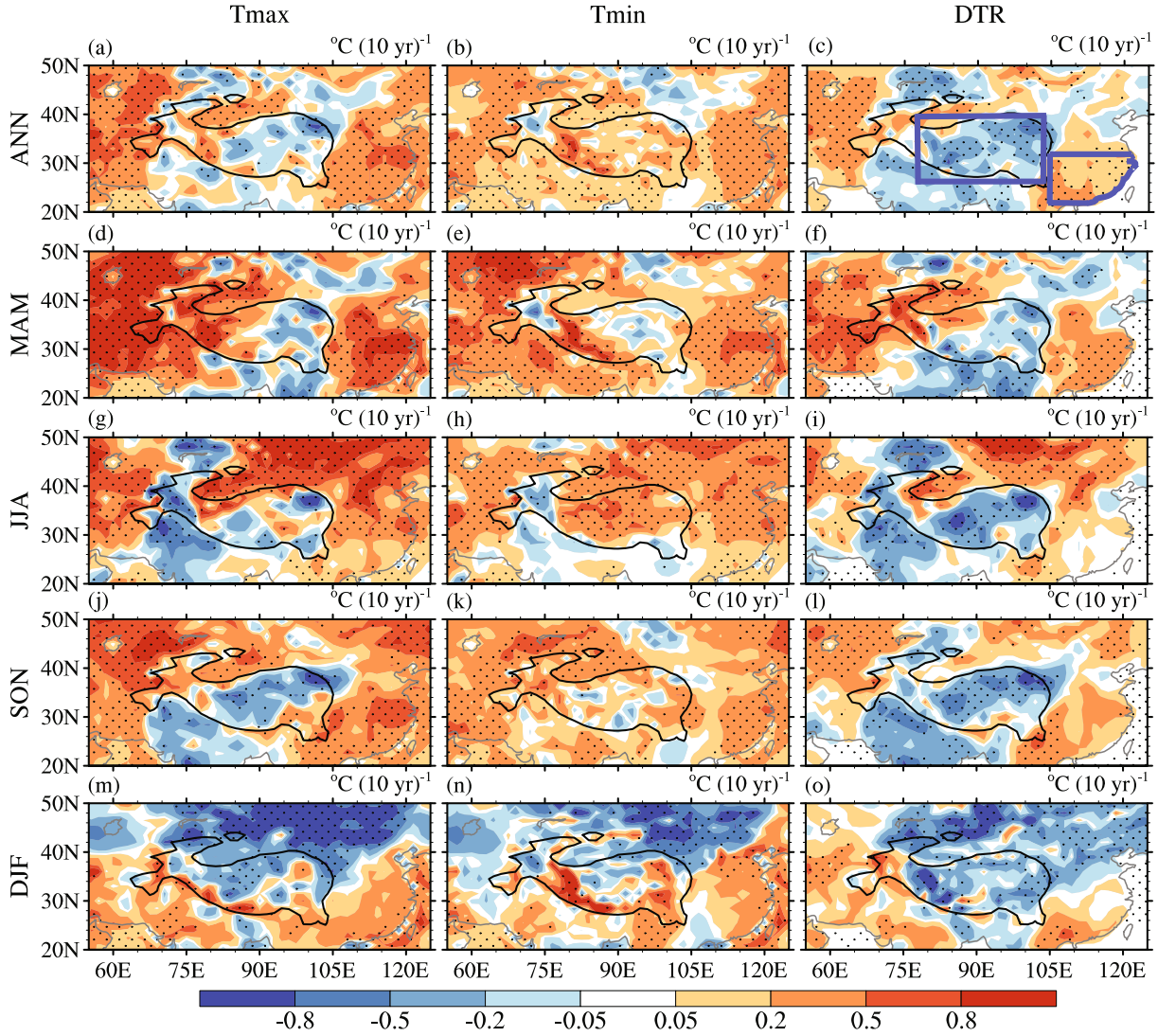

Fig. 2. Spatial distribution of the linear trend [units: °C (10 yr)$^{-1}$] of the annual mean (a) Tmax, (b) Tmin and (c) DTR during 1979–2012. (d–o) As in (a–c) but for (d–f) MAM, (g–i) JJA, (j–l) SON and (m–o) DJF. Dotted areas mark the 95% confidence level of significance according to the *t*-test. Blue boxes in (c) denote the TP and southeastern China areas for calculation of area-average respectively, the black solid contour in Fig. 2 and figures below denote the Tibetan Plateau.

Tmax than Tmin over southeastern China is related to the increase in the DTR—especially over South China, where the increase is up to 0.8°C.

In order to validate that CFRAM can successfully reproduce the observed temperature changes between the 2000s and 1980s, we display in Figs. 3d and e the total changes in Tmax and Tmin, respectively, as the sum of the partial temperature changes obtained from Eq. (4), and in Fig. 3f the DTR changes as the difference between Figs. 3d and e. Comparing Figs. 3a–c with Figs. 3d–f, it is evident that the spatial distributions as well as the magnitudes of the temperature changes obtained through CFRAM closely resemble those directly observed, thus confirming that the linearization of the energy perturbation in CFRAM is highly reliable and accurate.

4.2. *Attribution of the DTR changes to individual processes through CFRAM*

4.2.1. *Tmax changes*

Figure 4 shows the partial Tmax changes obtained in CFRAM, respectively due to the changes in the radiative processes including CO_2 concentration, surface albedo, cloud and water vapor, and the changes in the non-radiative processes including surface sensible heat flux, surface latent heat flux and the dynamic processes at the surface and in the atmosphere. Generally, the partial Tmax changes due to changes in the radiative processes are weaker than those due to changes in the non-radiative processes. Specifically, the partial Tmax changes due to changes in CO_2 concentration and surface albedo generally contribute to a warming pattern

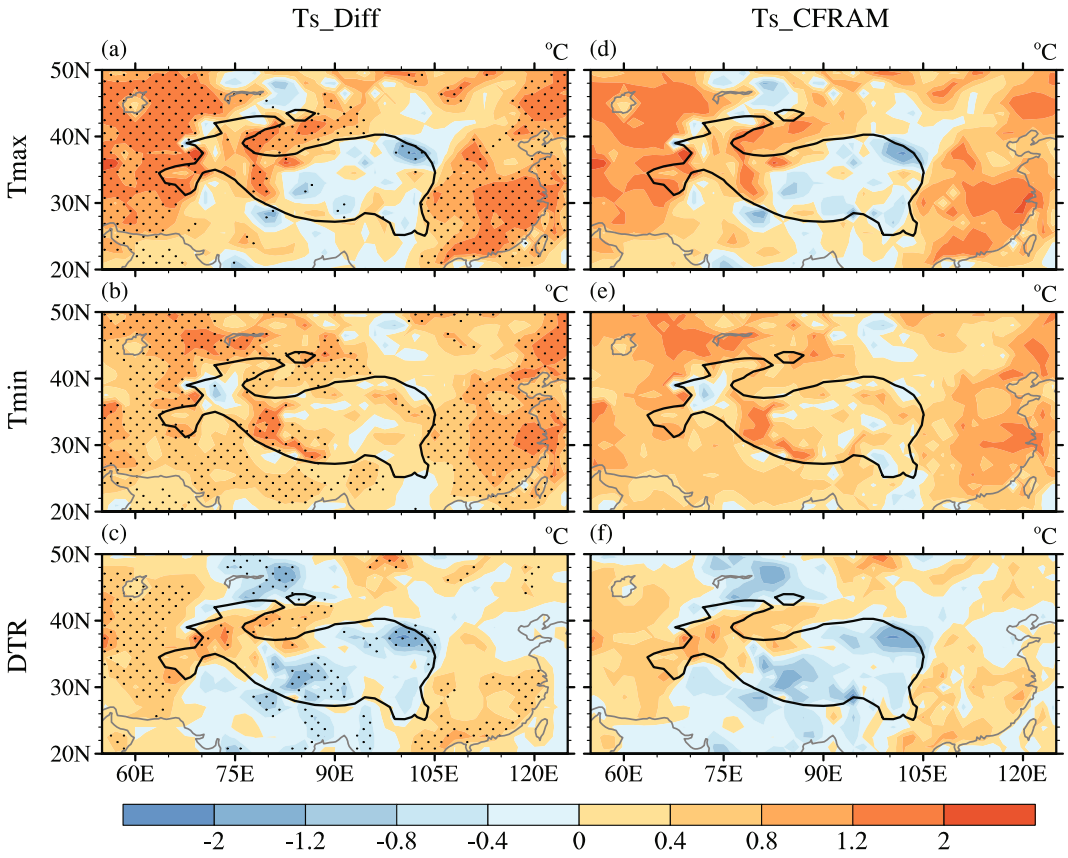

Fig. 3. Difference in the annual mean (a) Tmax, (b) Tmin and (c) DTR (units: °C) between the 2000s (2000–09 mean) and the 1980s (1980–89 mean). Dotted areas in (a–c) mark the 95% confidence level of significance according to the *t*-test. (d–f) As in (a–c) but for the sum of all the partial temperature changes obtained from CFRAM decomposition.

over both the TP and southeastern China, but are even weaker (<0.5°C) than those due to changes in cloud and water vapor (Figs. 4a and b vs. Figs. 4c and d). The partial Tmax changes due to cloud cover changes act to cool down the Tmax over the TP but warm up the Tmax over southeastern China. The cloud-induced cooling over the TP reaches its maximum (up to −8°C) over the southern boundary of the TP domain, while the warming amplitudes over southeastern China are within 5°C. The partial contributions from water vapor changes are much weaker (approximately ±0.5°C), and exhibit a generally opposite pattern to those from the cloud changes (Fig. 4c vs. 4d). From the total Tmax changes (Fig. 3a), it is clear that the cloud cover change during daytime is the main radiative feedback process contributing to the cooling/warming Tmax over the TP/southeastern China.

Although the partial contributions from the non-radiative processes are stronger than those from the radiative processes, they tend to counteract each other, particularly the surface sensible heat flux and dynamic processes (Fig. 4e vs. 4g). The latent heat flux changes act to cool down the Tmax over southeastern China, counteracting the dynamic processes (Fig. 4f vs. 4g); meanwhile, they cool down the Tmax over the southeastern part of the TP, counteracting the sensible heat flux changes (Fig. 4e vs. 4f). It is clear that the changes in dynamic processes are the main non-radiative contributor to the cooling/warming Tmax over the TP/southeastern China, which is co-contributed over the TP but counteracted over southeastern China by the latent heat flux changes, and is always counteracted by the sensible heat flux changes.

4.2.2. *Tmin changes*

Different from that for the Tmax changes, the partial Tmin changes due to non-radiative processes are weaker. Their magnitudes are comparable with those due to radiative processes, indicating the increased importance of radiative feedbacks during nighttime. Nevertheless, as with Tmax, the radiative warming contributions from the CO_2 and surface albedo to the Tmin are also less than 0.5°C (Figs. 5a and b). It can be seen that the general warming/cooling radiative contributions from the cloud and water vapor changes over the TP/southeastern China are largely compensated for by non-radiative processes (Figs. 5c and d vs. Figs. 5e–g), except that the latent heat flux changes over southeastern China tend to contribute to the Tmin cooling induced by radiative processes (Fig. 5f). This corresponds to the relatively weaker/stronger

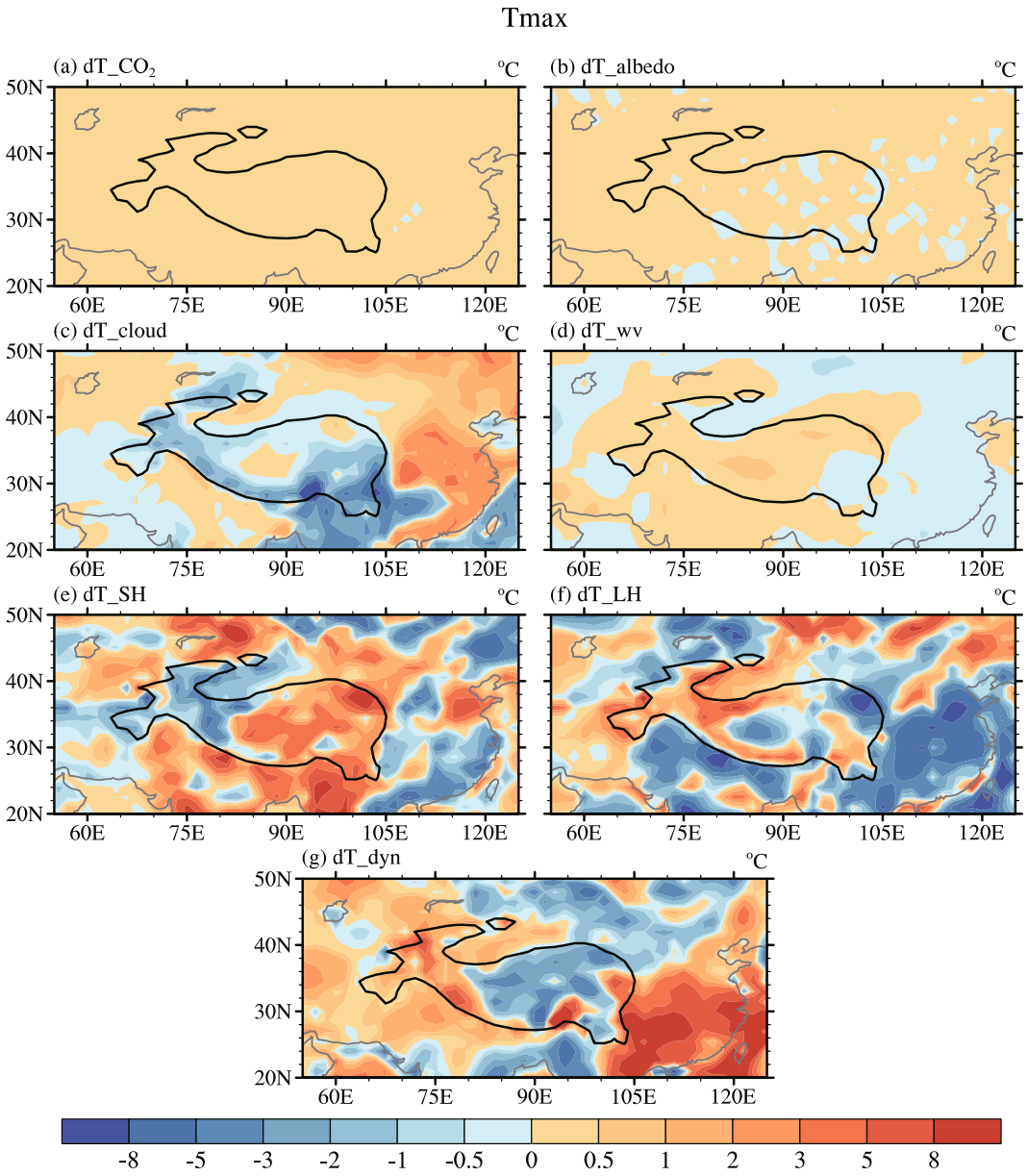

Fig. 4. Partial surface Tmax changes (units: °C) attributed to the changes in partial radiative processes including (a) CO_2 concentration, (b) surface albedo, (c) cloud, (d) water vapor; and non-radiative processes including (e) surface sensible heat flux, (f) surface latent heat flux and (g) dynamic processes at the surface and in the atmosphere, obtained from CFRAM decomposition.

Tmin warming over the TP/southeastern China (Fig. 3b). In addition, the non-radiative contributions from the dynamic processes are relatively larger than those from the surface heat flux changes (Figs. 5e–g), indicating the more important role played by dynamic processes for the Tmin changes during nighttime.

4.2.3. *DTR changes*

From the differences between Figs. 4 and 5, we derive the partial contributions of individual processes to the DTR changes, which are displayed in Fig. 6. From Fig. 3c, it is clear that the decreased/increased DTR over the TP/southeastern China is largely determined by the changes in radiative processes, particularly the cloud and water vapor feedbacks, as well as the changes in dynamic processes. Surface sensible heat flux feedbacks mainly compensate for the DTR changes over both the TP and southeastern China, while the surface latent heat flux feedbacks mitigate the DTR increase over southeastern China but enhance the DTR decrease over the TP. In addition, it is clear that the partial non-radiative contributions to the DTR changes mainly result from the changes in non-radiative processes during daytime, especially the surface heat flux processes, as indicated by the much larger magnitudes during daytime than during

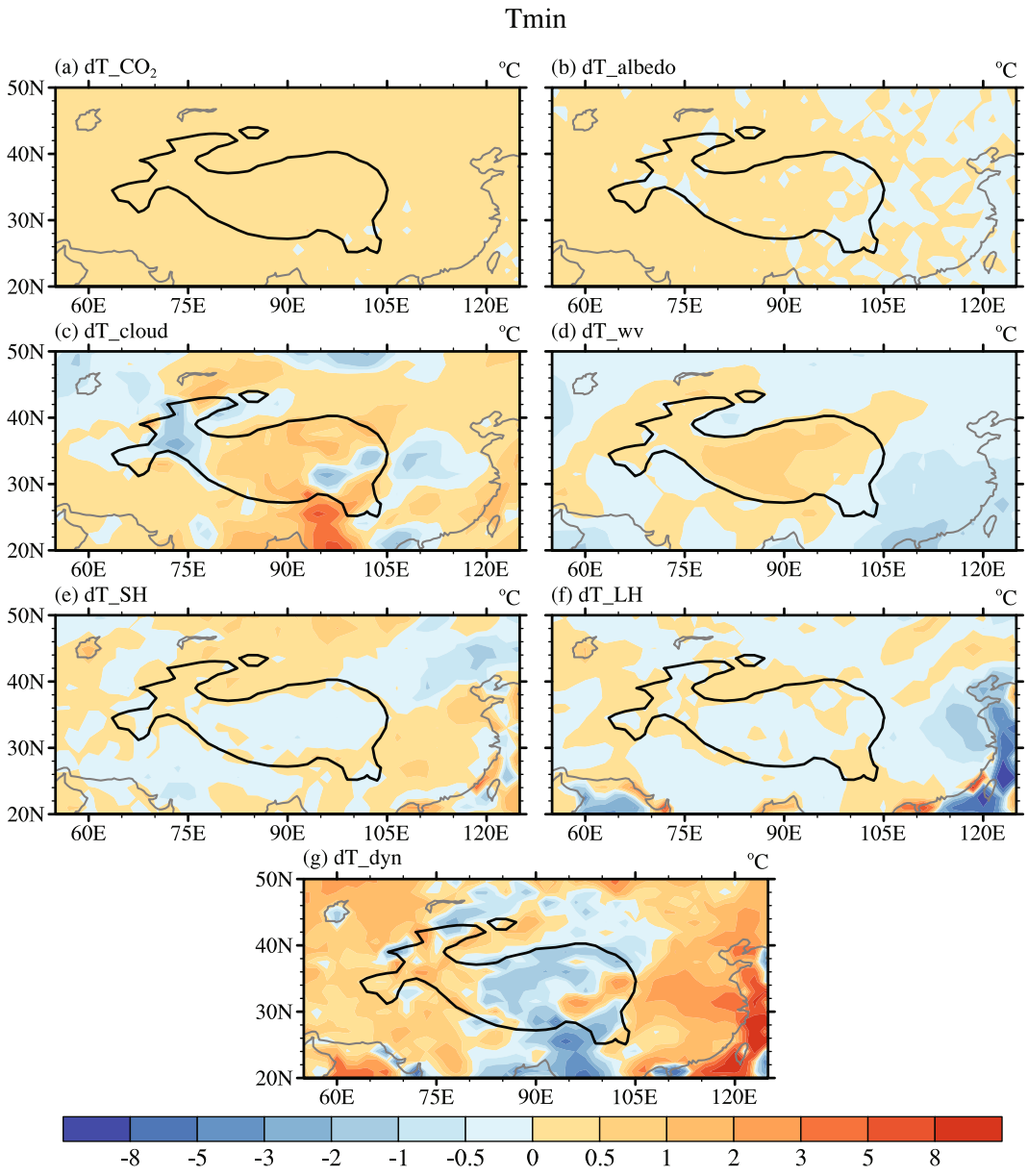

Fig. 5. As in Fig. 4 but for the surface Tmin.

nighttime (Figs. 4e and f vs. Figs. 5e and f).

4.3. *Understanding the main contributing processes for the DTR changes over the TP and southeastern China*

With regard to the relatively weaker contributions from CO_2 and surface albedo, we next provide further evidence to demonstrate the contributing processes of the related changes in cloud cover, water vapor content and surface heat fluxes, for the DTR changes.

4.3.1. *Cloud cover*

Previous studies have suggested that the changes in low-level cloud cover, rather than those in total cloud cover, are closely related to the long-term DTR changes over the TP (Duan et al., 2006; You et al., 2016). Hence, we first show the climatological mean low-level cloud amount (Figs. 7a and b) in the 1980s and its changes (Figs. 7c and d) between the 2000s and 1980s during daytime and nighttime, respectively. Compared with the 1980s, a consistent increase in the low-level cloud amount in the 2000s during daytime (Fig. 7c) is found across the entire TP, particularly over the southern part of the TP, with a significant increase up to 0.16; the cloud increase over the TP during nighttime is much weaker and confined to the central part of the TP. Meanwhile, low-level cloud cover over southeastern China has decreased during both daytime and nighttime, with the decrease being slightly stronger during nighttime.

Since the energy perturbations by cloud changes involve

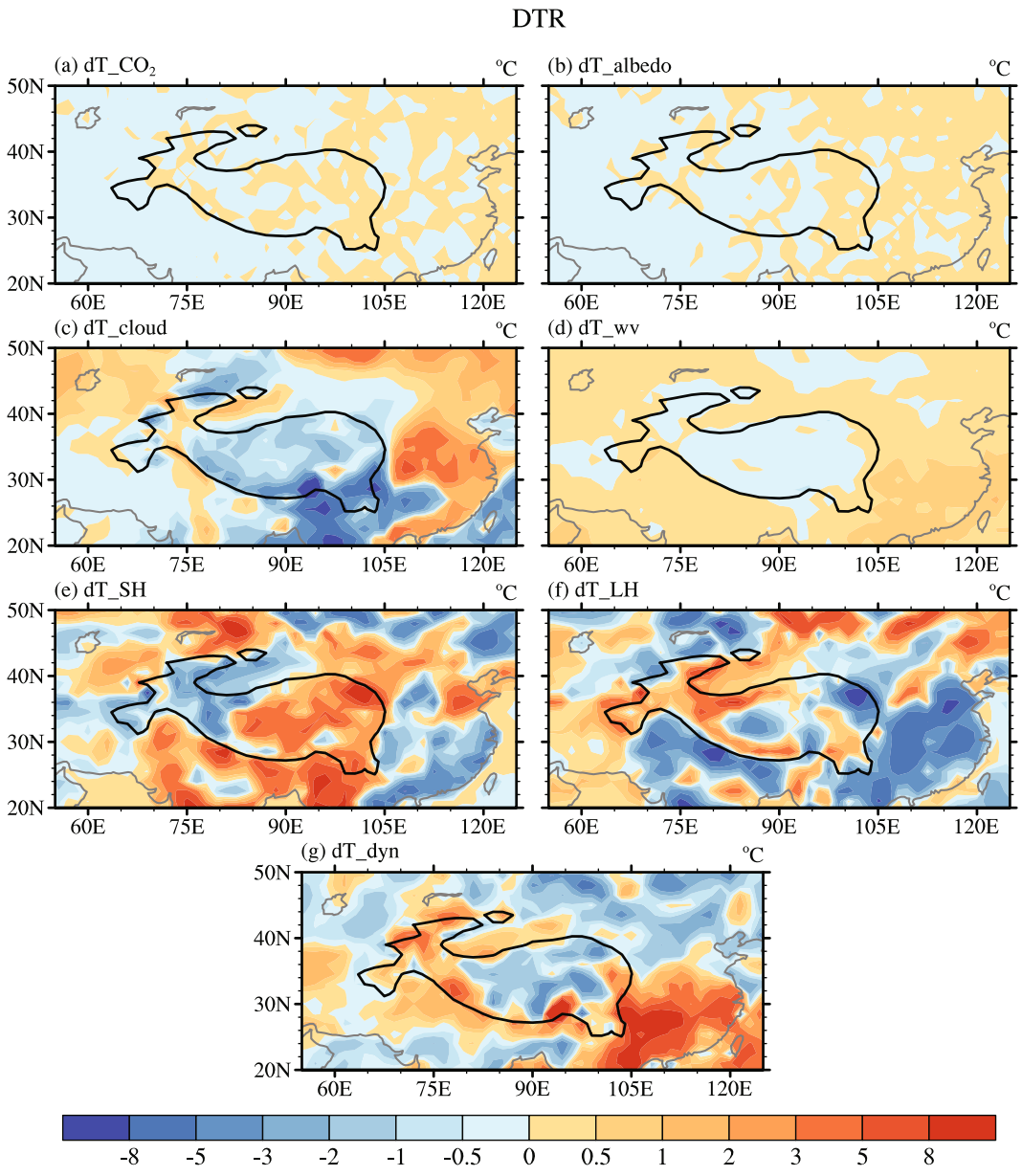

Fig. 6. As in Fig. 4 but for the DTR.

both shortwave and longwave radiative effects that tend to be opposite, next we separately examine the partial temperature changes associated with shortwave and longwave radiation effects. It can be seen from Fig. 7e that a cooling/warming effect on the Tmax exists over the TP/southeastern China during daytime (up to ±4°C), due to the strengthened/weakened blocking of downward shortwave radiation by the increased/decreased cloud cover. Whereas, the longwave radiative effect is largely opposite, due to the strengthened/weakened downward reflection of longwave radiation by the increased/decreased cloud cover over the TP/southeastern China during daytime (Fig. 7g). The overall Tmax changes due to cloud feedback changes are the balance between the shortwave and longwave radiative effects of cloud, the pattern of which is generally dominated by the shortwave effect of cloud (Fig. 7i).

The similar cloud cover changes during nighttime have yielded similar thermal effects to those during daytime, but with smaller magnitudes (within ±2°C) in relation to the much weaker cloud cover changes during nighttime (Figs. 7f and h). Unlike those during daytime, the longwave radiative effects of cloud changes tend to dominate the shortwave effects during nighttime, due to the lack of solar insolation. Overall, the cloud changes lead to a warming/cooling effect on the Tmin over the TP/ southeastern China (Fig. 7j).

With the largely opposite patterns of the temperature changes between Tmax and Tmin, the DTR changes due to cloud changes are considerably different (up to ±4°C) in

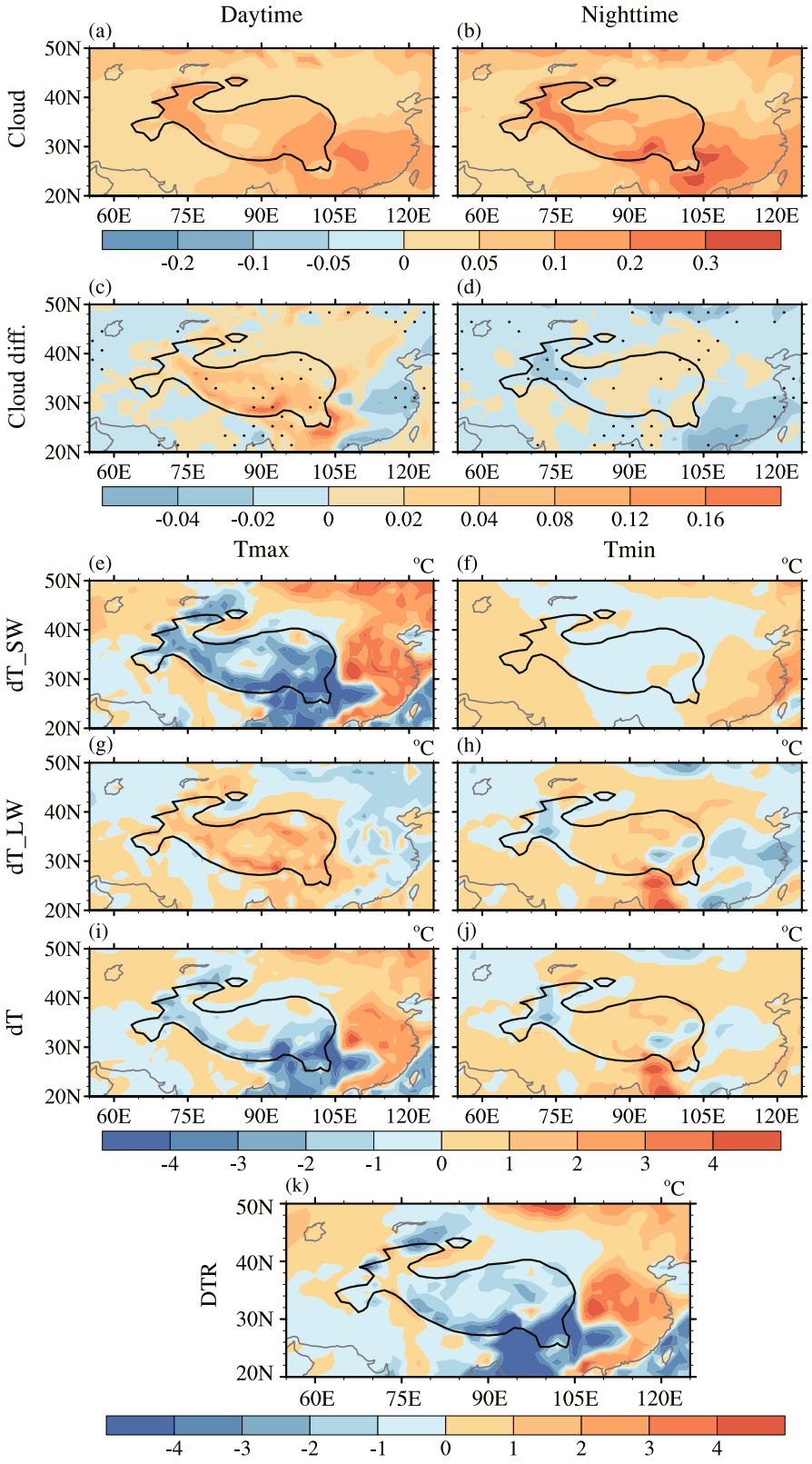

Fig. 7. (a, b) Climatology of the low-level cloud amount in the 1980s and (c, d) the differences between the 2000s and the 1980s, respectively, during (a, c) daytime and (b, d) nighttime. (e–j) Partial changes of (e, g, i) the Tmax and (f, h, j) the Tmin (units: °C) that are attributed to cloud (e, f) shortwave and (g, h) longwave radiation feedbacks, and (i, j) the total cloud feedbacks due to cloud changes. (k) DTR changes due to the changes in cloud feedback. Dotted areas in (c, d) mark the 95% confidence level of significance according to the *t*-test.

terms of the decreased DTR over the TP and the increased DTR over southeastern China (Fig. 7k). Comparing Figs. 7i and j, the cloud-induced Tmax changes and Tmin changes are both important for the DTR decrease/increase over the TP/southeastern China, except that the amplitudes of Tmin warming seem relatively larger than those of the Tmax cooling over the TP, and those of the Tmax warming are larger than those of the Tmin cooling over southeastern China. Consistent with this finding, Duan and Wu (2006) also emphasized the larger contributions of the warming effects due to the increased low-level cloud to the DTR decrease over the TP. Comparing Figs. 7e–h with Fig. 7k, we further propose that the cloud-induced decrease/increase in the DTR over the TP/southeastern China is mainly dominated by the shortwave radiative effect of cloud changes.

4.3.2. *Atmospheric water vapor*

As one of the most important greenhouse gases, atmospheric water vapor mainly absorbs longwave radiation from the surface and re-emits part of the radiation back to warm the surface. It can be seen from Figs. 8a and b that water vapor mainly concentrates in low latitudes and lower layers during both daytime and nighttime. Specifically, the column-accumulated water vapor content over the TP varies from 3 kg m^{-2} to 10 kg m^{-2} and increases southeastward and southward. Water vapor content over southeastern China (exceeding 20 kg m^{-2}) is more than two times that over the TP. From the 1980s to the 2000s, the atmospheric water vapor content increases by up to 0.5 kg m^{-2} over most parts of the TP during both daytime and nighttime, especially over the central and northeast TP; however, it decreases dramatically by up to −2.5 kg m^{-2} over southeastern China (Figs. 8c and d). The increased atmospheric water vapor over the TP is in accordance with the increased precipitable water vapor [0.14 mm $(10\ yr)^{-1}$] during recent decades (1976–2010) identified by Liang (2012) from radiosonde observation data. The partial changes of Tmax and Tmin due to water vapor changes closely follow the spatial patterns of water vapor changes, and always exhibit warming/cooling changes where water vapor increases/decreases (Figs. 8e and f). However, the relatively weaker Tmax warming than Tmin warming over the TP, due to the weaker/stronger increase in water vapor during daytime/nighttime, has resulted in the decreased DTR over the TP due to water vapor changes (Fig. 8g). On the contrary, the weaker-than-Tmin cooling of Tmax induced by water vapor changes over southeastern China, despite the slightly weaker decrease in water vapor during nighttime, has resulted in the increased DTR there (Fig. 8g), probably because of the more efficient greenhouse effect at night.

4.3.3. *Surface sensible heat flux*

It can be seen from Fig. 9a that the annual mean surface sensible heat flux (upward positive) is consistently positive (upward) during daytime, and is centered over the northeast TP (up to 200 W m^{-2}). The sensible heat flux over the TP is slightly stronger than that over southeastern China. Compared to the 1980s, the surface sensible heat flux during the 2000s is generally lower (by up to −20 W m^{-2}) over the TP, except the western TP region, but higher (by approximately 15 W m^{-2}) over southeastern China (Fig. 9c), indicating decreased/increased upward heat transport from the surface to the atmosphere during daytime over the TP/southeastern China. This is in agreement with the changes observed over the TP during 1980–2008 [approximately −19.8 W m^{-2} $(10\ yr)^{-1}$] (Wang et al., 2012). Correspondingly, the partial Tmax changes due to surface sensible heat flux are generally positive/negative over the TP/southeastern China, with maximum warming (approximately 8°C) over the central and northeast TP and maximum cooling (approximately -5°C) over the coastal region of southeastern China (Fig. 9e).

However, the surface Tmin changes during nighttime are so weak that the magnitudes are within ±1°C, due to the much weaker sensible heat flux and its changes during nighttime (Figs. 9d and f). As a result, the DTR changes due to changes in surface sensible heat flux are dominated by the Tmax changes during daytime, exhibiting increased/decreased DTR over the TP/southeastern China.

4.3.4. *Surface latent heat flux*

The surface latent heat flux is on average also much stronger during daytime than during nighttime, but both are positive (upward) during daytime and nighttime (Figs. 10a and b). The magnitudes of the surface latent heat flux during daytime generally decrease northward, and are thus much larger over southeastern China than over the TP (Fig. 10a). From the 1980s to the 2000s, the surface latent heat flux during daytime increases consistently over southeastern China (by up to 25 W m^{-2}), and also in the central and northeast TP region (Fig. 10c). This can be explained by the consistent increase in evaporation over southeastern China and the central and northeast TP region (approximately 0.2 mm) (Fig. 10e). As a result, the increased evaporation, and thus the elevated latent heat transportation to the atmosphere, during daytime over these regions, corresponds to the cooling changes of Tmax (over −8°C); meanwhile, over other regions, the Tmax is mostly positive (Fig. 10g).

However, Tmin changes are much smaller, relatively, than those of Tmax (Fig. 10h), in relation to the much weaker latent heat flux and its changes during nighttime (Figs. 10b, d and f). Therefore, the DTR changes due to changes in surface latent heat flux are mainly determined by the Tmax changes, showing a consistently decreased DTR over southeastern China and the central and northeast TP region (up to −8°C).

4.3.5. *Quantifying the relative importance based on area-mean contributions to the DTR changes*

To further quantify the relative contribution to the long-term changes of DTR from individual processes, we calculate the area-averaged (blue boxes in Fig. 2c) partial changes in Tmax, Tmin and DTR over the TP and southeastern China, for the annual mean and four seasons separately. Firstly, it is clear from Figs. 11a and f that the annual mean magnitudes of the partial Tmax changes are relatively larger than those

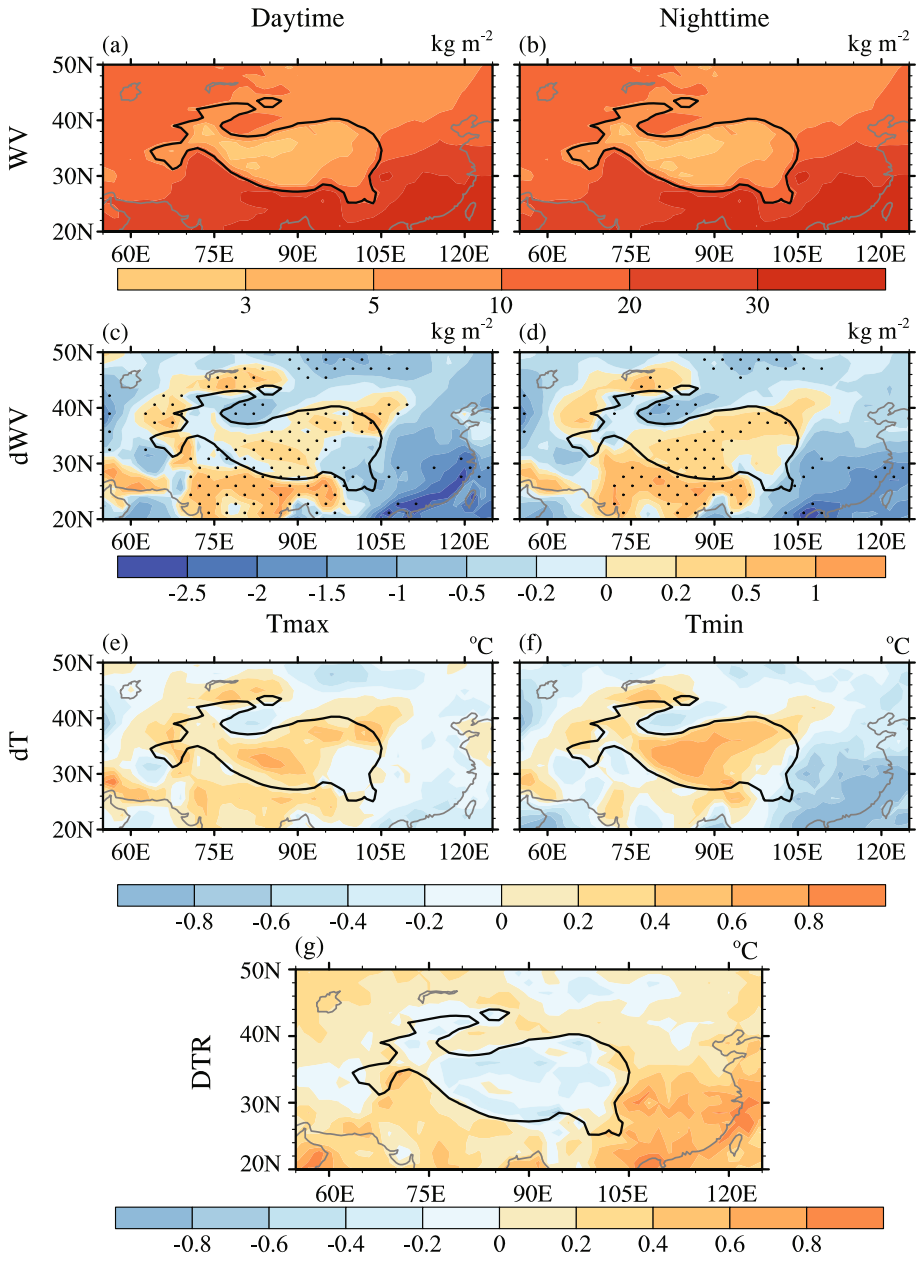

Fig. 8. (a, b) Climatology of the column water vapor content (units: kg m^{-2}) in the 1980s and (c, d) the differences between the 2000s and the 1980s, respectively, during (a, c) daytime and (b, d) nighttime. (e–g) Partial changes in (e) Tmax, (f) Tmin and (g) DTR (units: °C) that are attributed to changes in water vapor feedback. Dotted areas in (c, d) mark the 95% confidence level of significance according to the *t*-test.

of Tmin over both the TP and southeastern China, indicating stronger surface–atmosphere coupling during daytime. In particular, the annual mean DTR over the TP has decreased by 0.43°C (Fig. 11a), which is contributed by the radiative processes (approximately −2°C) and compensated for by the non-radiative processes (approximately 1.6°C). Specifically, the increase in cloud cover becomes the dominant contributor to the decreased DTR by cooling/warming the Tmax/Tmin over the TP, which is co-contributed by the stronger Tmin warming than Tmax warming due to the increased atmospheric water vapor over the TP, as well as the stronger Tmax cooling due to the changes in surface latent heat flux and dynamic processes. Although surface latent heat flux and dynamic processes contribute to the decreased DTR over the northeast and central TP locally (Figs. 2f and g), they tend to contribute to increasing the DTR over the south TP. This leads to the area-averaged DTR changes over the TP being mainly dominated by the changes in cloud, since changes in cloud contribute to decreasing the DTR over the whole TP. The decreased DTR over the TP is mitigated by the stronger

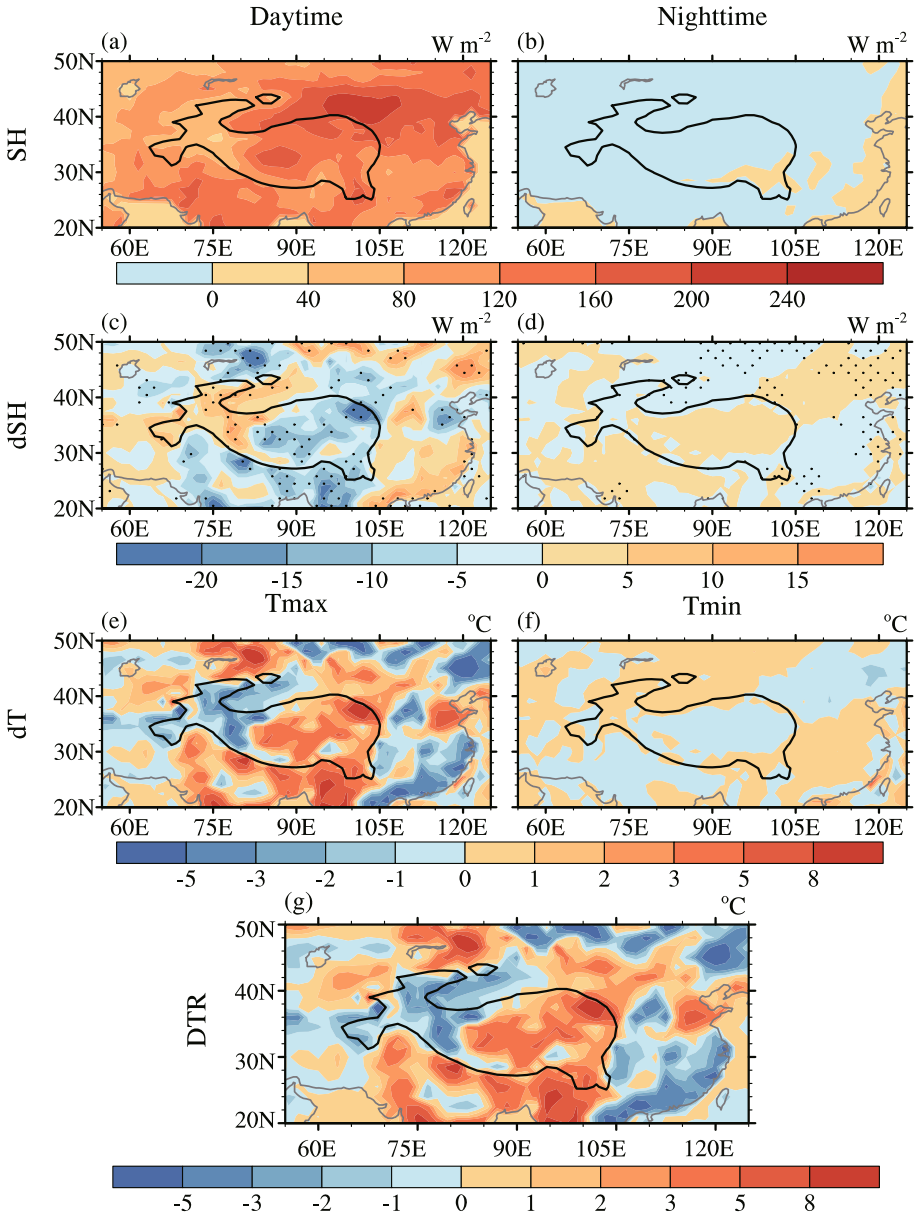

Fig. 9. As in Fig. 8 but for surface sensible heat flux (units: W m^{-2}).

Tmax warming due to the reduction of upward surface sensible heat flux over TP. Furthermore, the decreased DTR over the TP exists in all seasons, and is relatively stronger in the cold seasons (−0.46 in DJF and −0.42 in SON) than in the warm seasons (−0.03 in MAM and −0.20 in JJA) (Figs. 11b–e). Consistent among all seasons except DJF, the decrease in the DTR is mainly contributed by the radiative processes, particularly cloud feedbacks, and is compensated for by the non-radiative processes. Non-radiative processes, including surface latent heat flux and dynamic processes, seem to be the main contributors for the decreased DTR over the TP during DJF.

Compared with the TP, the amplitudes of the contributions from individual processes to the DTR changes are much larger over southeastern China, and are approximately twice those over the TP (Figs. 11f–j). The total DTR changes, however, are still comparable between the TP and southeastern China. Specifically, the long-term increase in the annual mean DTR over southeastern China (0.39°C) is mainly contributed by radiative processes, including cloud and water vapor feedbacks, while the non-radiative processes act to decrease the DTR because of the considerable cancelling out between the strong Tmax cooling caused by the increased upward surface sensible heat flux and surface evaporation, and the strong Tmax warming caused by dynamic processes (Fig. 11f). As for the long-term changes in the seasonal mean DTR over southeastern China, the increased DTR in all seasons except SON is somehow mainly contributed by non-radiative

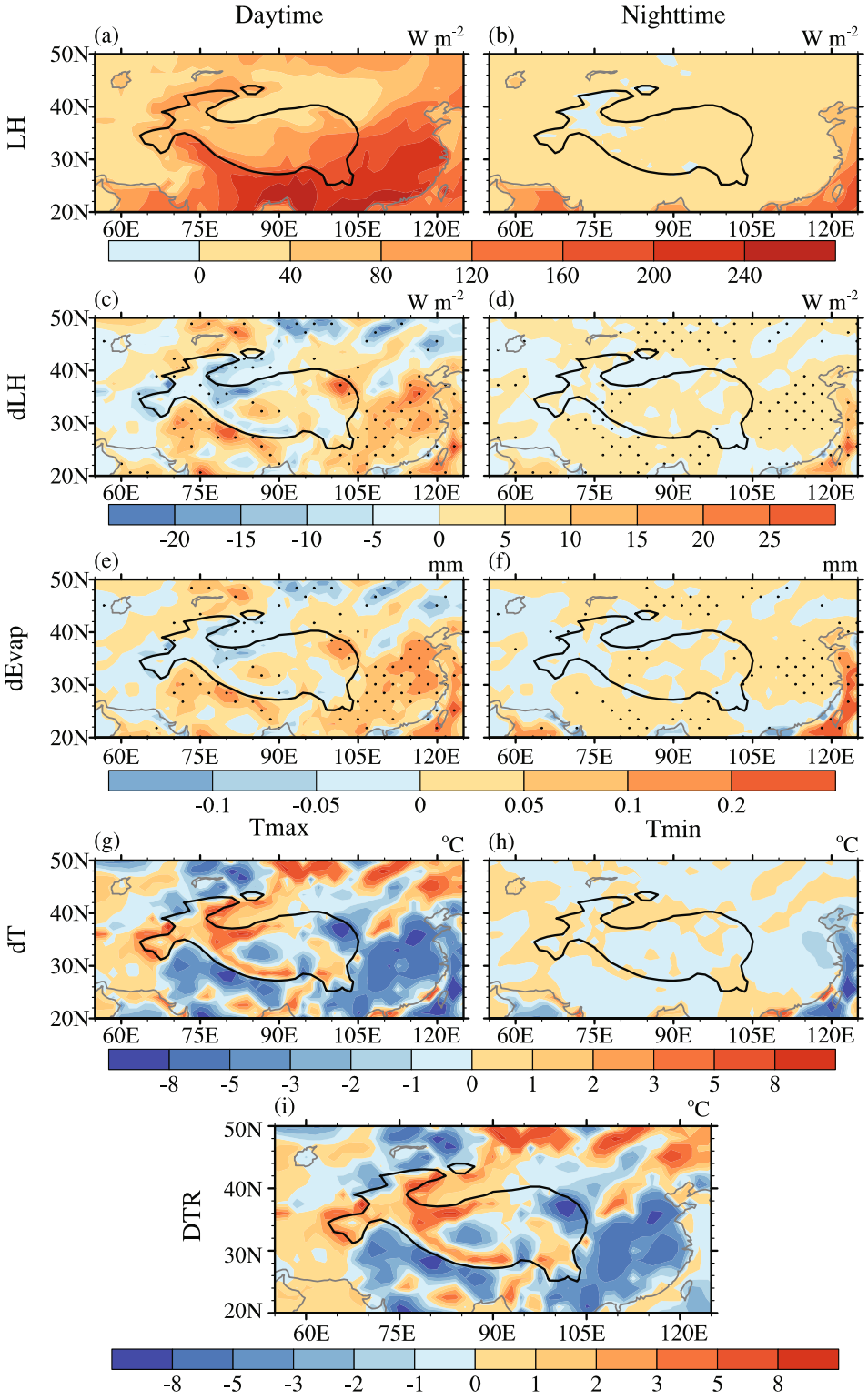

Fig. 10. (a, b) Climatology of the surface latent heat flux (units: W m^{-2}) in the 1980s and (c, d) the differences between the 2000s and the 1980s, respectively, during (a, c) daytime and (b, d) nighttime. (e, f) Differences in evaporation (units: mm) between the 2000s and the 1980s during (e) daytime and (f) nighttime. (g–i) Partial changes in (g) Tmax, (h) Tmin and (i) DTR (units: °C) that are attributed to changes in surface latent heat flux. Dotted areas in (c–f) mark the 95% confidence level of significance according to the *t*-test.

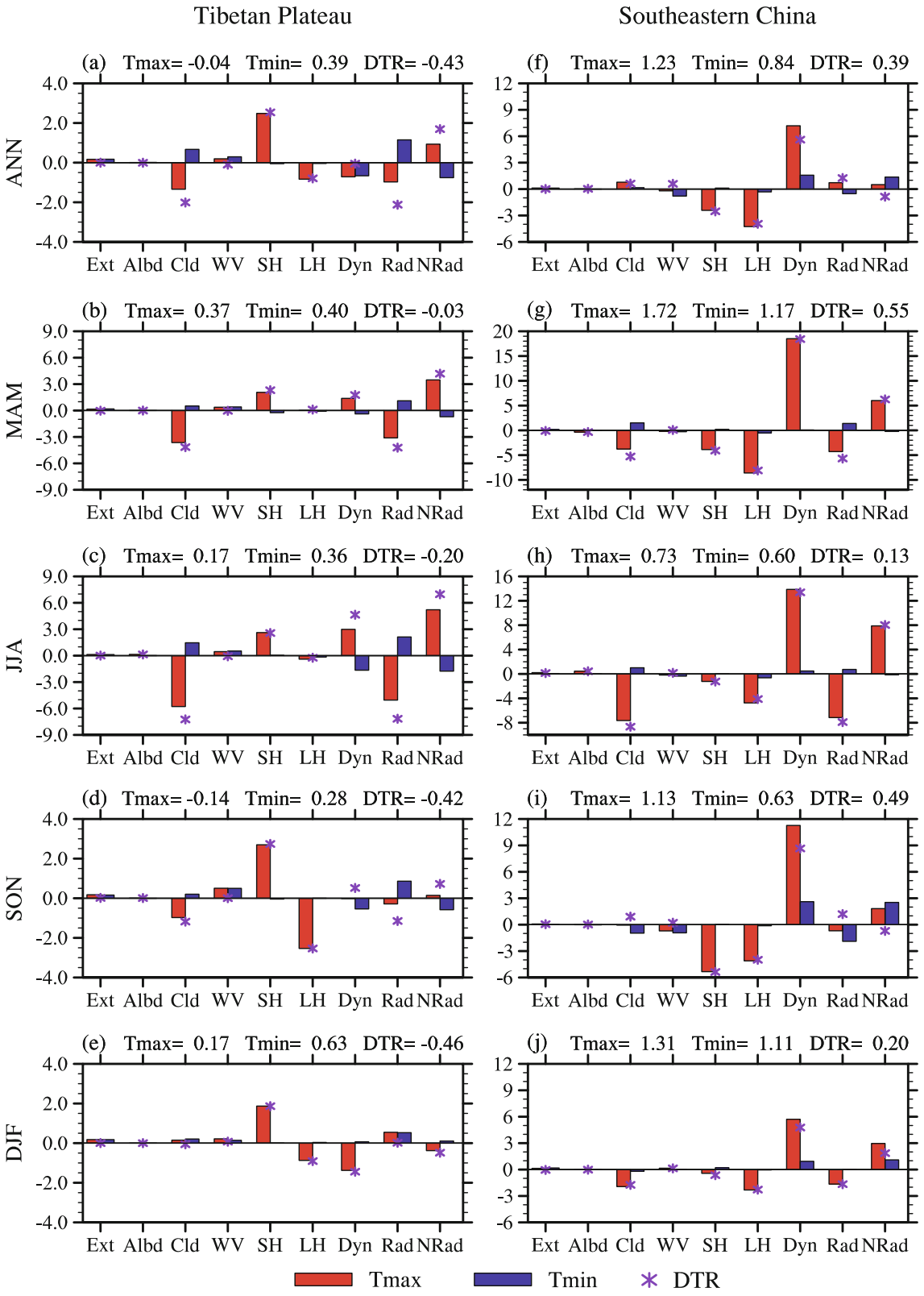

Fig. 11. (a) Area-averaged annual mean partial temperature changes (units: °C) of Tmax (red bars), Tmin (blue bars) and DTR (purple stars) attributed to changes in CO_2, surface albedo, cloud, water vapor, surface sensible heat flux and latent heat flux, surface and atmospheric dynamic processes, the sum of radiative processes, and the sum of non-radiative processes, respectively, over the Tibetan Plateau. (b–e) As in (a) but for (b) MAM, (c) JJA, (d) SON and (e) DJF. (f–j) As in (a–e) but over southeastern China.

processes as a balance between the Tmax warming due to dynamic processes and the Tmax cooling due to increased surface heat fluxes as well as cloud feedbacks (Figs. 11g, h and j).

5. Concluding remarks

This study analyzes the different long-term changes in the DTR over the TP and southeastern China since the 1980s, based on ERA-Interim reanalysis data. The results indicate that the decreased DTR over the TP results from a strong Tmin warming combined with a weak Tmax cooling. The most significant decrease in DTR is found in the winter season. However, it is found that the DTR over southeastern China has increased particularly during MAM, and has mainly resulted from the stronger Tmax than Tmin warming.

By applying a process-based decomposition method (CFRAM), the physical processes responsible for the long-term changes in the DTR are analyzed quantitatively. It is indicated that the decreased DTR over the TP is mainly contributed by radiative processes (exceeding −2°C); particularly, the Tmax/Tmin cooling/warming due to the increases in low-level cloud cover (approximately −2°C), as well as the Tmin warming due to the increased atmospheric water vapor during nighttime (approximately −0.4°C). Changes in non-radiative processes (approximately 1.6°C), which are balanced by the stronger/weaker increased surface latent heat flux (approximately −0.8°C) and the stronger/weaker decreased surface sensible heat flux (∼ 2.5°C) during daytime/nighttime and dynamic processes (approximately −0.4°C), act to partially compensate for the DTR decrease by radiative processes. In contrast, the increased DTR over southeastern China is co-contributed by changes in cloud, water vapor and dynamic processes. Unlike that over TP, the low-level cloud cover over southeastern China has decreased, leading to the Tmax warming via shortwave radiative feedback and the Tmin cooling via longwave radiative feedback. Atmospheric water vapor has also decreased, which contributes to the increased DTR by the stronger Tmin than Tmax cooling. Meanwhile, changes in surface sensible and latent heat fluxes act to mitigate the increase in DTR through stronger Tmax than Tmin cooling.

In general, this study not only confirms the decrease in the DTR over the TP in the ERA-Interim data, but also indicates contrasting long-term changes in the DTR between the TP and southeastern China. We further perform a quantitative decomposition analysis of the DTR changes to demonstrate the physical mechanisms responsible for the DTR changes over the East Asian region. However, it should be noted that DTR changes in urban regions may also be influenced by changes in land-use associated with urbanization (Price et al., 1999; Kalnay and Cai, 2003), which is not explicitly considered in this study due to the coarse spatial resolution of the ERA-Interim dataset. Meanwhile, due to the lack of layer-by-layer distribution fields of other minor gases (e.g. aerosols) in ERA-Interim, their radiative effects are not explicitly demonstrated in the current version of CFRAM, but are considered implicitly in the effects of dynamic processes. Nevertheless, to fully understand the mechanisms responsible for the DTR changes, further diagnosis of the changes in the atmospheric circulation is obviously needed, as well as a more comprehensive radiative model for CFRAM. For example, Duan and Wu (2008) indicated the weakening of the thermal forcing of the TP is associated with a weakening of the wind speed over the TP. Nevertheless, the information provided in this study is still valuable for future investigations.

Acknowledgements. This work was jointly supported by the China Meteorological Administration Special Public Welfare Research Fund (Grant No. GYHY201406001), the National Natural Science Foundation of China (Grant Nos. 91437105, 41575041 and 41430533), and Special Foundation for National Commonweal Institutes of China (Grant No. IUMKY201614).

REFERENCES

Braganza, K., D. J. Karoly, and J. M. Arblaster, 2004: Diurnal temperature range as an index of global climate change during the twentieth century. *Geophys. Res. Lett.*, **31**, doi: 10.1029/2004GL019998.

Cai, M., and J. H. Lu, 2009: A new framework for isolating individual feedback processes in coupled general circulation climate models. Part II: Method demonstrations and comparisons. *Climate Dyn.*, **32**, 887–900.

Cai, M., and K. K. Tung, 2012: Robustness of dynamical feedbacks from radiative forcing: 2% solar versus $2\times CO_2$ experiments in an idealized GCM. *J. Atmos. Sci.*, **69**, 2256–2271.

Collatz, G. J., L. Bounoua, S. O. Los, D. A. Randall, I. Y. Fung, and P. J. Sellers, 2000: A mechanism for the influence of vegetation on the response of the diurnal temperature range to changing climate. *Geophys. Res. Lett.*, **27**(20), 3381–3384.

Dai, A. G., K. E. Trenberth, and T. R. Karl, 1999: Effects of clouds, soil moisture, precipitation, and water vapor on diurnal temperature range. *J. Climate*, **12**, 2451–2473.

Decker, M., M. A. Brunke, Z. Wang, K. Sakaguchi, X. B. Zeng, and M. G. Bosilovich, 2012: Evaluation of the reanalysis products from GSFC, NCEP, and ECMWF using flux tower observations. *J. Climate*, **25**(6), 1916–1944.

Dee, D. P., and Coauthors, 2011: The ERA-Interim reanalysis: Configuration and performance of the data assimilation system. *Quart. J. Roy. Meteor. Soc.*, **137**, 553–597.

Deng, Y., T. W. Park, and M. Cai, 2012: Process-based decomposition of the global surface temperature response to El Niño in boreal winter. *J. Atmos. Sci.*, **69**, 1706–1712.

Duan, A. M., and G. X. Wu, 2005: Role of the Tibetan Plateau thermal forcing in the summer climate patterns over subtropical Asia. *Climate Dyn.*, **24**(7), 793–807.

Duan, A. M., and G. X. Wu, 2006: Change of cloud amount and the climate warming on the Tibetan plateau. *Geophys. Res. Let.*, **33**, 217–234.

Duan, A. M., and G. X. Wu, 2008: Weakening trend in the atmospheric heat source over the Tibetan Plateau during recent decades. Part I: Observations. *J. Climate*, **21**, 3149–3164.

Duan, A. M., and Z. X. Xiao, 2015: Does the climate warming hiatus exist over the Tibetan Plateau? *Sci. Rep.*, **5**, 13711, doi: 10.1038/srep13711.

Duan, A. M., G. X. Wu, Q. Zhang, and Y. M. Liu, 2006: New proofs of the recent climate warming over the Tibetan Plateau as a result of the increasing greenhouse gases emissions. *Chinese Science Bulletin*, **51**, 1396–1400.

Easterling, D. R., and Coauthors, 1997: Maximum and minimum temperature trends for the globe. *Science*, **277**, 364–367.

Fu, Q., and K. N. Liou, 1992: On the correlated *k*-distribution method for radiative transfer in nonhomogeneous atmospheres. *J. Atmos. Sci*., **49**, 2139–2156.

Fu, Q., and K. N. Liou, 1993: Parameterization of the radiative properties of cirrus clouds. *J. Atmos. Sci*., **50**, 2008–2025.

Kalnay, E., and M. Cai, 2003: Impact of urbanization and land-use change on climate. *Nature*, **423**, 528–531.

Kang, S. C., Y. W. Xu, Q. L. You, W.-A. Flügel, N. Pepin, and T. D. Yao, 2010: Review of climate and cryospheric change in the Tibetan plateau. *Environ. Res. Lett*., **5**(1), 015101.

Karl, T. R., and Coauthors, 1993: Asymmetric trends of daily maximum and minimum temperature. *Bull. Amer. Meteor. Soc*., **74**, 1007–1023.

Liang, H., 2012: Variation of the Atmospheric water vapor and its radiative effect simulation over the Tibetan Plateau. PhD dissertation, Chinese Academy of Meteorological Sciences. (in Chinese)

Liu, B. H., M. Xu, M. Henderson, Y. Qi, and Y. Q. Li, 2004: Taking China's temperature: Daily range, warming trends, and regional variations, 1955–2000. *J. Climate*, **17**, 4453–4462.

Liu, B., T. J. Zhou, and J. H. Lu, 2015: Quantifying contributions of model processes to the surface temperature bias in FGOALS-g2. *Journal of Advances in Modeling Earth Systems*, **7**, 1519–1533.

Liu, X. D., and B. D. Chen, 2000: Climatic warming in the Tibetan Plateau during recent decades. *Int. J. Climatol*., **20**(14), 1729–1742.

Lu, J. H., and M. Cai, 2009: A new framework for isolating individual feedback processes in coupled general circulation climate models. Part I: Formulation. *Climate Dyn*., **32**, 873–885.

Mao, J. F., X. Y. Shi, L. J. Ma, D. P. Kaiser, Q. X. Li, and P. E. Thornton, 2010: Assessment of reanalysis daily extreme temperatures with China's homogenized historical dataset during 1979-2001 using probability density functions. *J. Climate*, **23**, 6605–6623.

Oku, Y., H. Ishikawa, S. Haginoya, and Y. M. Ma, 2006: Recent trends in land surface temperature on the Tibetan Plateau. *J. Climate*, **19**, 2995–3003.

Park, T.-W., Y. Deng, M. Cai, J.-H. Jeong, and R. J. Zhou, 2014: A dissection of the surface temperature biases in the community earth system model. *Climate Dyn*., **43**(7–8), 2043–2059.

Price, C., S. Michaelides, S. Pashiardis, and P. Alpert, 1999: Long term changes in diurnal temperature range in Cyprus. *Atmos Res.*, **51**(2), 85–98.

Ren, G. Y., and Y. Q. Zhou, 2014: Urbanization effect on trends of extreme temperature indices of national stations over Mainland China, 1961–2008. *J. Climate*, **27**, 2340–2360.

Ren, R. C., G. X. Wu, M. Cai, S. Y. Sun, X. Liu, and W. P. Li, 2014: Progress in research of stratosphere-troposphere interactions: Application of isentropic potential vorticity dynamics and the effects of the Tibetan Plateau. *Journal of Meteorological Research*, **28**(5), 714–731.

Ren, R. C., Y. Yang, M. Cai, and J. Rao, 2015: Understanding the systematic air temperature biases in a coupled climate system model through a process-based decomposition method. *Climate Dyn*., **45**(7–8), 1801–1817.

Ren, R. C., S. Y. Sun, Y. Yang, and Q. Li, 2016: Summer SST anomalies in the Indian Ocean and the seasonal timing of ENSO decay phase. *Climate Dyn*., **47**, 1827–1844, doi: 10.1007/s00382-015-2935-0.

Sejas, S. A., M. Cai, A. X. Hu, G. A. Meehl, W. Washington, and P. C. Taylor, 2014: Individual feedback contributions to the seasonality of surface warming. *J. Climate*, **27**(14), 5653–5669.

Shen, X. J., B. H. Liu, G. D. Li, Z. F. Wu, Y. H. Jin, P. J. Yu, and D. W. Zhou, 2014: Spatiotemporal change of diurnal temperature range and its relationship with sunshine duration and precipitation in China. *J. Geophys. Res*., **119**, 13 163–13 179.

Shi, Q., and S. Liang, 2014: Surface-sensible and latent heat fluxes over the Tibetan Plateau from ground measurements, reanalysis, and satellite data. *Atmos. Chem. Phys*., **14**, 5659–5677.

Stone, D., and A. Weaver, 2003: Factors contributing to diurnal temperature range trends in twentieth and twenty-first century simulations of the CCCma coupled model. *Climate Dyn*., **20**(5), 435–445.

Sun, Y. T., Q. J. Gao, and J. Z. Min, 2013: Comparison of reanalysis data and observation about summer/winter surface air temperature in Tibet. *Plateau Meteorology*, **32**, 909–920 (in Chinese).

Wang, A. H., and X. B. Zeng, 2012: Evaluation of multireanalysis products with in situ observations over the Tibetan Plateau. *J. Geophys. Res*., **117**, D05102.

Wang, M. R., S. W. Zhou, and A. M. Duan, 2012: Trend in the atmospheric heat source over the central and eastern Tibetan Plateau during recent decades: Comparison of observations and reanalysis data. *Chinese Science Bulletin*, **57**, 548–557.

Wang, Z. Q., A. M. Duan, and G. X. Wu, 2014: Time-lagged impact of spring sensible heat over the Tibetan Plateau on the summer rainfall anomaly in east China: Case studies using the WRF model. *Climate Dyn*., **42**(11), 2885–2898.

Wu, G. X., and Coauthors, 2007: The influence of mechanical and thermal forcing by the Tibetan Plateau on Asian Climate. *Journal of Hydrometeorology*, **8**, 770–789.

Wu, G. X., Y. M. Liu, B. He, Q. Bao, A. M. Duan, and F.-F. Jin, 2012: Thermal controls on the Asian summer monsoon. *Sci. Rep*., **2**, 404, doi: 10.1038/srep00404.

Xia, X., 2013: Variability and trend of diurnal temperature range in China and their relationship to total cloud cover and sunshine duration. *Ann. Geophys*., **31**, 795–804.

Yanai, M., and G.-X. Wu, 2006: Effects of the Tibetan Plateau. B. Wang, Ed., *The Asian Monsoon*, Springer, Berlin Heidelberg, 513–549.

Yang, K., H. Wu, J. Qin, C. G. Lin, W. J. Tang, and Y. Y. Chen, 2014: Recent climate changes over the Tibetan plateau and their impacts on energy and water cycle: A review. *Global and Planetary Change*, **112**, 79–91.

Yang, Y., and R.-C. Ren, 2015: Understanding the global surface-atmosphere energy balance in FGOALS-s2 through an attribution analysis of the global temperature biases. *Atmos. Ocean. Sci. Lett*., **8**, 107–112.

Yang, Y., R. C. Ren, M. Cai, and J. Rao, 2015: Attributing analysis on the model bias in surface temperature in the climate system model FGOALS-s2 through a process-based decomposition method. *Adv. Atmos. Sci*., **32**, 457–469, doi: 10.1007/s00376-014-4061-z.

Yang, Y., R.-C. Ren, and M. Cai, 2016: Towards a physical understanding of stratospheric cooling under global warming through a process-based decomposition method. *Climate Dyn*., doi: 10.1007/s00382-016-3040-8.

You, Q. L., S. C. Kang, E. Aguilar, and Y. P. Yan, 2008: Changes in daily climate extremes in the eastern and central Tibetan Plateau during 1961–2005. *J. Geophys. Res*., **113**, D07101, doi: 10.1029/2007JD009389.

You, Q. L., K. Fraedrich, J. Z. Min, S. C. Kang, X. H. Zhu, G. Y. Ren, and X. H. Meng, 2013: Can temperature extremes in China be calculated from reanalysis? *Global and Planetary Change*, **111**, 268–279.

You, Q. L., J. Z. Min, Y. Jiao, M. Sillanpää, and S. C. Kang, 2016: Observed trend of diurnal temperature range in the Tibetan Plateau in recent decades. *International Journal of Climatology*, 36, 2633–2643, doi: 10.1002/joc.4517.

Zhou, L. M., R. E. Dickinson, A. G. Dai, and P. Dirmeyer, 2010: Detection and attribution of anthropogenic forcing to diurnal temperature range changes from 1950 to 1999: Comparing multi-model simulations with observations. *Climate Dyn*., **35**, 1289–1307.